Clays and Clay Minerals, Vol. 69, No. 1:142–151, 2021

FABRICATION OF ANTHOCYANIN/MONTMORILLONITE HYBRID PIGMENTS TO ENHANCE THEIR ENVIRONMENTAL STABILITY AND APPLICATION IN ALLOCHROIC COMPOSITE FILMS

Shu E. Li[1,2,3], B. Mu[1,3,*], Jun J. Ding[1,3], H. Zhang[1,2,3], Xiao W. Wang[1,3], and Ai Q. Wang[1,3,*]

[1] Key Laboratory of Clay Mineral Applied Research of Gansu Province, Center of Eco-Materials and Green Chemistry, Lanzhou Institute of Chemical Physics, Chinese Academy of Sciences, Lanzhou 730000, P. R. China
[2] Center of Materials Science and Optoelectronics Engineering, University of Chinese Academy of Sciences, Beijing 100049, P. R. China
[3] Center of Xuyi Palygorskite Applied Technology, Lanzhou Institute of Chemical Physics, Chinese Academy of Sciences, Xuyi 211700, P. R. China

Abstract—The poor environmental stability of natural anthocyanin hinders its usefulness in various functional applications. The objectives of the present study were to enhance the environmental stability of anthocyanin extracted from *Lycium ruthenicum* by mixing it with montmorillonite to form an organic/inorganic hybrid pigment, and then to synthesize allochroic biodegradable composite films by incorporating the hybrid pigment into sodium alginate and test them for potential applications in food testing and packaging. The results of X-ray diffraction, Fourier-transform infrared spectroscopy, and use of the Brunauer–Emmett–Teller method and zeta potential demonstrated that anthocyanin was both adsorbed on the surface and intercalated into the interlayer of montmorillonite via host–guest interaction, and the hybrid pigments obtained allowed good, reversible, acid/base behavior after exposure to HCl and NH_3 atmospheres. The composite films containing hybrid pigments had good mechanical properties due to the uniform dispersion of the pigments in a sodium alginate substrate and the formation of hydrogen bonds between them. Interestingly, the composite films also exhibited reversible acidichromism. The as-prepared hybrid pigments in composite films could, therefore, serve simultaneously as a reinforced material and as a smart coloring agent for a polymer substrate.

Keywords—Anthocyanin · Environmental stabilities · Hybrid pigments · Intelligent composite films · Montmorillonite

INTRODUCTION

Food safety is of the utmost importance in society. Food-safety accidents not only cause suffering, due to food poisoning, but also lead to food waste which exerts pressure on the environment (Kuswandi and Nurfawaidi 2017). Accordingly, exploring the materials used to monitor the levels of food safety and prevent resource waste is very important. At present, three types of smart materials have been applied widely for determining the freshness of food, i.e. intelligent films (Cao et al. 2019; Pereira et al. 2015; Zhai et al. 2017), sensors (Puligundla et al. 2012; Zhai et al. 2019), and pH indicators (Choi et al. 2017; Kuswandi and Nurfawaidi 2017; Maciel et al. 2015). The application of these materials in food packaging and testing provides a convenient means for consumers to assess the freshness and quality of food by means of a color response by the smart materials (Müller and Schmid 2019; Pereira et al. 2015; Realini and Marcos 2014). Novel colorimetric films are applied for intelligent food packaging, real-time monitoring of meat freshness, and detection of milk spoilage (Fang et al. 2017; Kuswandi et al. 2012; Liu et al. 2017; Mihindukulasuriya and Lim 2014; Silvestre et al. 2011). Smart films have recently attracted increasing attention in various fields due to good color-changing properties and physicochemical characteristics.

Anthocyanin (ACN) is a water-soluble flavonoid pigment with a variety of bright colors depending on the acidity or alkalinity of the environment, which is mainly related to the existence of phenolic or conjugated substances and the number of hydroxyl and methyl groups (Ma and Wang 2016; Riaz et al. 2016; Li et al. 2019a,b). The ACN is, therefore, introduced into agar/potato starch, chitosan/corn starch, and chitosan/polyvinyl alcohol films used to develop intelligent packaging materials (Choi et al. 2017; Koosha and Hamedi 2019; Qin et al. 2019; Silva-Pereira et al. 2015). Taking into account the instability of these natural pigments in relation to external factors, e.g. light, oxygen, and temperature, improving the resistance of ACN to the external environment is crucial. At present, the most common method is to confine the natural pigments in an inorganic host. Composites possessing good photostability were obtained by immobilizing ACN on Al- and Fe-containing mesoporous silica (Kohno et al. 2014, 2015). In addition, clay minerals (e.g. saponite, palygorskite, and sepiolite) were also used to adsorb ACN for constructing hybrid pigments with reversible allochroic behavior and good weathering resistance (Ogawa et al. 2017; Li et al. 2019a; Silva et al. 2019). Recently, a series of hybrid pigments with excellent chemical and thermal stability was

* E-mail address of corresponding author: mubin@licp.cas.cn; aqwang@licp.cas.cn
DOI: 10.1007/s42860-021-00114-z

fabricated successfully by anchoring ACN on different types of clay minerals (Li et al. 2019b).

Montmorillonite (Mnt) is a 2:1 clay mineral belonging to the smectite group which has been used widely as an inorganic matrix for improving the stability of cationic dyes, owing to its crystal structure and permanent negative charge (Chiou and Rutherford 1997; Ferrage 2016; Luo et al. 2019; Xie et al. 2001). Several pigment molecules, such as thioindigo, carminic acid, and alizarin, were immobilized on Mnt substrates to design hybrid materials with good stability and improved levels of performance (Guillermin et al. 2019; Ramírez et al. 2011; Trigueiro et al. 2018). The clay minerals, especially Mnt, also led to a reinforced effect on organic/inorganic composite films. For example, Mnt is applied as the reinforcement and color stabilizer in gelatin films containing acerola juice (Ribeiro et al. 2018a,b). Monmorillonite might, therefore, be a promising host material for loading of natural pigments to be used in composite films with reversible allochroic behaviors and mechanical properties.

The goals of the present study were to 'fabricate intelligent' allochroic sodium alginate composite films by introducing various amounts of ACN/Mnt hybrid pigments into the composite, then to investigate the effects of acidic and alkaline atmospheres on the color, chemical and thermal performance, and mechanical and allochroic properties of the hybrid pigments in the biodegradable composite films.

MATERIALS AND METHODS

Materials

Montmorillonite (Mnt) was obtained from Jianping Wanxing Bentonite Co. Ltd., Chaoyang, China. The raw Mnt was treated using 4% HCl (wt.%) (Sichuan Xilong Chemical Co. Ltd, Chengdu, China) and then filtered by passing through a 200-mesh sieve for removal of the associated carbonates and silica sand. The main chemical components of Mnt were Al_2O_3 13.79%, Na_2O 1.21%, MgO 8.10%, CaO 2.21%, SiO_2 56.99%, K_2O 0.22%, and Fe_2O_3 3.14%, as measured using an E3 X-ray fluorescence spectrometer (PANalytical, Almelo, The Netherlands). The ripe fruits of *Lycium ruthenicum* were provided by the Linhai Biotechnology Development Co., Ltd., Baiyin, China. Sodium alginate (SA) was purchased from Xilong Chemical Factory Co., Ltd., Guangzhou, China.

Preparation of ACN/Mnt Hybrid Pigments

The ACN was extracted from *Lycium ruthenicum* using a modification of the technique described by Wang et al. (2018): the fruit was ground in a mortar without damaging the seeds, 1 g of which was then added to 75 g of deionized water (the pH was adjusted to 1.98 with 0.1 M HCl), and the mixture was sonicated (KQ-250DB, Kunshan Ultrasonic Instrument Co., Ltd., Kunshan, China) at 70°C for 90 min. After that, Mnt (2 g) was added slowly to the sonicated ACN extract to achieve a solid-to-liquid ratio of 1:60 and stirred magnetically for 24 h at room temperature. The solid produced was separated by centrifugation (TDL-5C, INESA, Shanghai, China) at 2300×*g* for 10 min followed by washing with 120 mL of distilled water, and then dried at 60°C for 2 h with the water content maintained at 40%. Finally, it was ground for 30 min and then heated at 120°C for 4 h.

Stability Tests of ACN/Mnt Hybrid Pigments

The ACN/Mnt powder (0.04 g) was immersed in 20 mL of 1 M HCl in ethanol (Li'an Longbohua Pharmaceutical Chemical Co., Ltd., Tianjin, China) for 24 h to evaluate the chemical stability. The above solutions were centrifuged at 2300×*g* for 10 min, and the solid obtained was dried in an oven (Shanghai Jinghong Experimental Equipment Co. Ltd., Shanghai, China) at 40°C. The chromaticity parameters of the dried sample were measured using a Color-Eye automatic differential colorimeter (X-Rite, Ci 7800, Pantone Inc., Carlstadt, New Jersey, USA).

Reversible Acid/Base Allochroic Behavior of ACN/Mnt Hybrid Pigments

The ACN/Mnt was exposed to an acidic or alkaline atmosphere derived from the volatilization of HCl and $NH_3{\cdot}H_2O$ (Kaitong Chemical Reagent Co. LTD, Tianjin, China) in closed desiccators. Firstly, the samples were placed in a desiccator containing HCl atmosphere for 6 min, and then transferred into another desiccator filled with an NH_3 atmosphere. The samples were transferred alternately from the acid atmosphere to the basic one, the corresponding color change was recorded with a camera, and the chromatic value of the hybrid pigments was measured after the color change experiment.

Preparation of ACN/Mnt/SA Smart Films

The ACN/Mnt/SA smart films were prepared by a solvent casting method (Li et al. 2019a). Firstly, SA (3 g) was dissolved in 147 g of distilled water at room temperature for 12 h under mechanical stirring to obtain a transparent solution (2 wt.%); 0.6 g glycerol (20 wt.% of the total mass of polymer weight) was added as a plasticizer, and then the solution was stirred continuously at room temperature until the solution became clear. Next, a 150 mL SA solution was mixed with various amounts of ACN/Mnt hybrid pigments, to reach 2%, 4%, or 6% of the total mass of the polymer; the total volume was fixed at 200 mL. Finally, the above mixture was poured into plastic petri dishes and dried at room temperature to form uniform films.

Evaluation of Acid-response Allochroic Behavior and Mechanical Properties of ACN/Mnt/SA Smart Films

In order to evaluate the allochroic behavior of smart films, the pure SA film and composite films with ACN/Mnt contents of 2, 4, and 6 wt.% were placed in a dryer filled with an HCl or NH_3 atmosphere to observe the color response. The four groups of films were transferred into another desiccator containing an NH_3 atmosphere after the color responses of samples to an HCl atmosphere had been observed and recorded.

https://doi.org/10.1007/s42860-021-00114-z Published online by Cambridge University Press

Tensile tests of composite films (length:width ratio = 8:1) were measured with a New SANS universal material testing system (CMT4304, Xinsansi Material Testing Co., Ltd, Shenzhen, China) equipped with a 200 Nload cell and 20 mm/min crosshead speed. All samples were kept in a desiccator at 55% relative humidity (RH) and room temperature for 72 h before characterization. The measurements of films were repeated five times and averaged.

Characterization Techniques

The X-ray diffraction (XRD) patterns were recorded using an X'pert Pro diffractometer (PANalytical Co., Almelo, The Netherlands) along with Cu-Kα radiation at 40 kV and 30 mA, the diffraction data of samples were over the range 3–80°2θ at a scanning speed of 2°2θ min^{-1}. The Fourier-transform infrared (FTIR) spectra of a series of powder samples were measured over the range 4000–400 cm^{-1} on a Nicolet NEXUS FTIR spectrometer (Nicolet iS50, Thermo Scientific, Waltham, Massachusetts, USA) using KBr pellets. The FTIR spectra of the films were recorded on a NEXUS 870 spectrometer (NEXUS 870, Thermo Nicolet, USA) using an attenuated total reflectance (ATR) accessory. The zeta potentials of hybrid materials were obtained from Malvern Zetasizer Nano system (ZEN3600, Malvern, UK) with 633 nm He–Ne laser irradiation. The morphologies of samples were observed using field emission scanning electron microscopy (FESEM, JSM-6701F, JEOL, Tokyo, Japan). The surface area and pore volume of samples were measured at –196ºC with N_2 as an adsorbate using the Accelerated Surface Area and Porosimetry System (Micromeritics, ASAP2020, Atlanta, Georgia, USA). The colorimetric values of all hybrid pigments were calculated on a Color-Eye automatic differential colorimeter (X-Rite, Ci 7800, Pantone Inc., Carlstadt, NJ, USA) according to the Commission Internationale de l'Eclairage $L^* a^* b^*$ colorimetric method: L^*(0-black/100-white), a^* (negative-green/positive-red), and b^* (negative-blue/positive-yellow). Thermal gravimetric analysis (TGA) was obtained using an STA449F3 simultaneous thermal analyzer (NETZSCH-Gerätebau GmbH, Berlin, Germany). The UV–vis spectra of the eluate were obtained using a TU-1900 UV-vis spectrometer (PERSEE, Beijing, China). UV-vis diffuse reflectance spectra were also collected using the X-Rite, Ci 7800 instrument.

RESULTS AND DISCUSSION

Characterization of ACN/Mnt Hybrid Pigments

The intercalation of natural ACN molecules into the interlayer of Mnt can be confirmed indirectly by the interlayer spacing of Mnt before and after adsorption of ACN according to XRD patterns (Fig. 1a). The d_{001} value of 13.74 Å at 6.43°2θ indicated that the raw Mnt was a mono-hydrated layer (Ferrage 2016). After incorporation of ACN, the value of d_{001} expanded slightly to 13.93 Å. The interlayer spacing of Mnt increased with increase in the number of organic guests (Kohno et al. 2009; Ribeiro et al. 2018a, b). In addition, no obvious changes were observed in the peak intensities of the (100), (110), (210), and (060) planes, indicating that the loading of ACN between interlayers of Mnt did not obviously destroy the crystal structure of Mnt (Zhang et al. 2015), which could also be confirmed by SEM images of Mnt before and after incorporation of ACN (Supplementary Material, Fig. S1).

Information about bonding and structural changes in the ACN guests and Mnt was obtained from the FTIR spectra (Fig. 1b). The characteristic band of Mnt at 3620 cm^{-1} was attributed to the stretching vibration of the structural –OH groups, which was related to the amount of octahedral Al (Madejová 2003). The bands at 3424 and 1638 cm^{-1} corresponded to the –OH stretching and bending vibrations of hydration water, respectively. The absorption bands at ~1038, 916, and 846 cm^{-1} could be due to the tetrahedral Si–O stretching vibration and the octahedral Al–Al–OH and Al–Mg-OH bending vibrations, respectively (Madejová

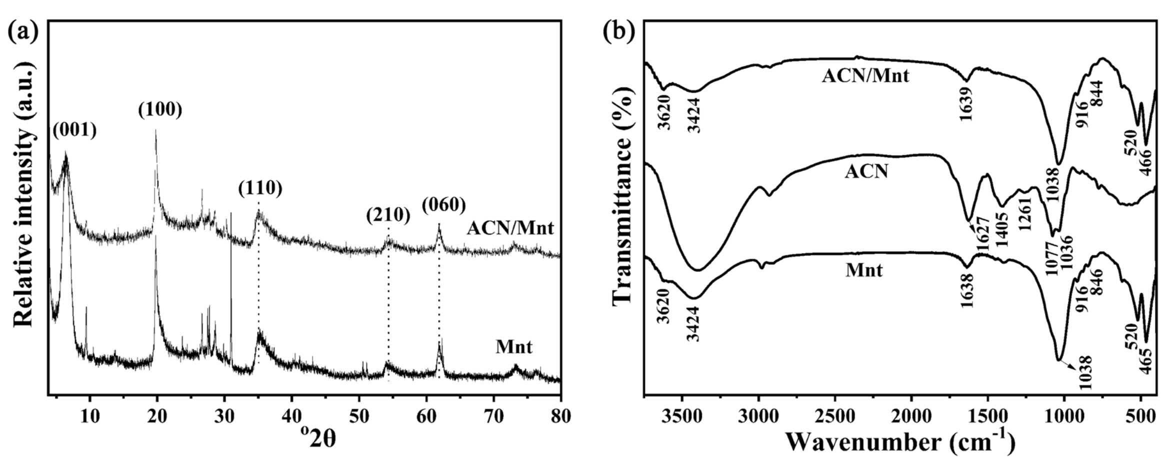

Fig. 1. **a** XRD patterns of Mnt and ACN/Mnt hybrid pigments and **b** FTIR spectra of Mnt, ACN, and ACN/Mnt

https://doi.org/10.1007/s42860-021-00114-z Published online by Cambridge University Press

Table 1. BET data and zeta potentials of the pure ACN, Mnt, and ACN/Mnt hybrid pigments

Samples	S_{BET} (m^2/g)	S_{ext} (m^2/g)	V_{total} (cm^3/g)	Zeta potentials (mV)
ACN	–	–	–	–29.33
Mnt	37.99	33.32	0.0858	–33.13
Mnt-G-30	34.41	35.34	0.0838	–21.47
ACN/Mnt	7.20	10.08	0.0189	–36.50

et al. 2017; Merino et al. 2016). The Si–O and Al–O bending vibrations were observed at ~520 and 465 cm^{-1}, respectively (Wang et al. 2017). The presence of ACN molecules was indicated by the appearance of bands in three regions centered at ~1627–1405, 1261, and 1627–1036 cm^{-1}. These bands were assigned to the C=C stretching vibration of aromatic compounds, to the pyran ring, and to C–H deformation in aromatic compounds, respectively (Zhai et al. 2017; Li et al. 2019a,b). These bands were absent from the FTIR spectrum of ACN/Mnt because of overlap with the absorption peaks of Mnt.

In order to investigate the effect of the preparation conditions on the pore structural parameters of Mnt, the specific surface area (S_{BET}), the external surface area (S_{ext}), and the total pore volume (V_{total}) of Mnt before and after grinding for 30 min (Mnt-G-30) were determined (Table 1). No significant changes were found, indicating that the grinding process had little influence on the structure of Mnt. In the case of ACN/Mnt hybrid pigments, S_{BET} and V_{total} of Mnt decreased, by 81.08 and 77.97%, respectively, after incorporation of ACN. The result suggested that some ACN molecules had been adsorbed on the surface of Mnt. In addition, the zeta potential of Mnt became less negative, from –33.13 to –21.47 mV after grinding, which was consistent with a previous report (Maqueda et al. 2013). The zeta potential of ACN was –29.33 mV, due to the predominant form of an anionic quinoidal structure in neutral deionized water (Fedenko et al. 2017; Kang et al. 2018; Ribeiro et al. 2018a,b). In order to evaluate the binding mode of ACN and Mnt during adsorption, the zeta potential values of ACN (6.89) and hybrid pigments (–14.43) were determined at pH 1.90 (Table S1). The zeta potential values indicated that ACN in the form of flavylium cations was bonded to negatively charged Mnt via electrostatic interaction during the adsorption process (Li et al. 2019a,b). Under neutral conditions, ACN molecules transformed from the flavylium cations to the quinoidal structure, resulting in significantly more negative (to –36.50 mV) zeta potentials of hybrid pigments measured in neutral deionized water.

Environmental Stability of ACN/Mnt Hybrid Pigments

Thermal stability. The thermal stabilities of ACN extracted from *Lycium ruthenicum*, Mnt, and ACN/Mnt hybrid pigments were compared by means of TGA curves (Fig. 2). The ACN presented two weight-loss steps in the temperature range from room temperature to 800°C; one step was due to evaporation of adsorbed water at <170°C and the other was related mainly to the degradation and carbonization of the ACN skeleton in a nitrogen atmosphere (Cai et al. 2019). In the case of Mnt, the mass loss

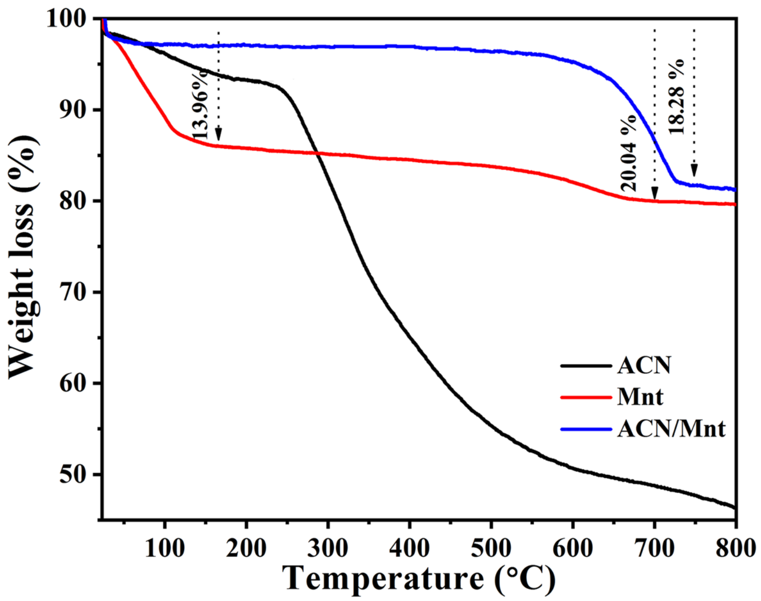

Fig. 2. TGA curves of ACN, Mnt, and ACN/Mnt hybrid pigments

https://doi.org/10.1007/s42860-021-00114-z Published online by Cambridge University Press

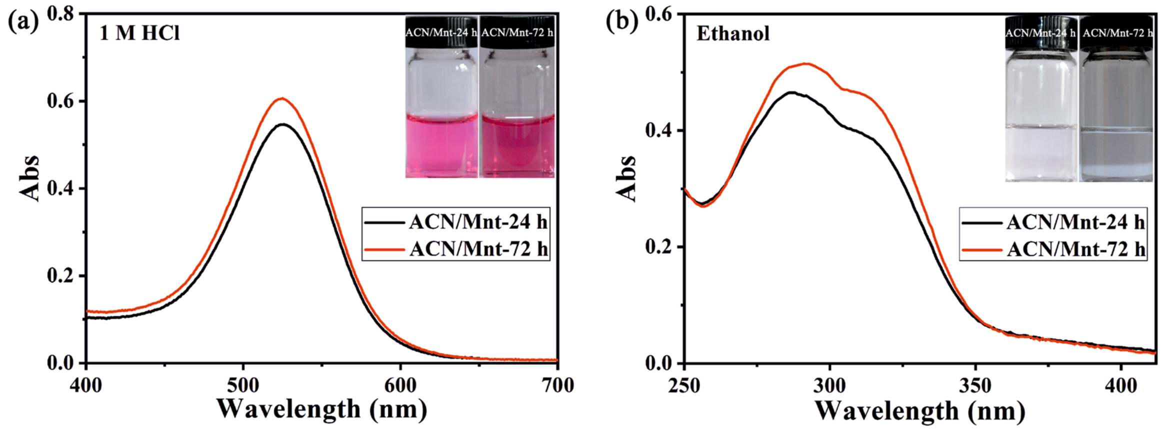

Fig. 3. UV-vis spectra and images of the supernatants of ACN/Mnt hybrid pigments following immersion in **a** 1 M HCl and **b** ethanol, for 24 and 72 h, respectively

of ~13.96% at low temperature (< 170°C) was attributed to the loss of physically adsorbed H_2O and interlayer water (Suchithra et al. 2012; Trigueiro et al. 2018). With increase in temperature, the mass loss of 6.08% was due to the dehydroxylation of Mnt (Gutiérrez et al. 2017; Wang et al. 2017). For the hybrid pigments, no obvious mass loss was observed below 150°C, compared with Mnt, which might be related to the heating treatment during the preparation process. In addition, significant mass losses (18.28%) of ACN/Mnt were observed in the temperature range ~500–750°C, corresponding to the removal of structural OH and the decomposition of ACN molecules (~12.20%) (Guillermin et al. 2019). The shielding effect of Mnt on ACN molecules could obviously improve the thermal stability of natural pigments, therefore, compared with the pure ones.

Chemical stability. Various solvents (1 M HCl and ethanol) were used to evaluate the chemical stability of the hybrid pigments following immersion for 24 h and 72 h, respectively (Fig. 3). The colors of the supernatants after acid and ethanol treatment were pink and colorless, respectively, accompanied by a shift in the characteristic absorption peaks from 526 to 286 and 291 nm. This phenomenon was ascribed to the structural transformation of ACN molecules from the flavylium cations to carbinol pseudobase (Castañeda-Ovando et al. 2009; Zhai et al. 2017; Li et al. 2019a,b). In addition, the absorbance of the supernatant after treatment with 1 M HCl for 24 and 72 h at 526 nm was 0.55 and 0.60, respectively. Likewise, the absorbance of the supernatant after ethanol erosion for 24 and 72 h at 286 nm was 0.47 and 0.51, respectively, indicating that the hybrid pigments exhibited excellent chemical resistance to acid and ethanol. In addition, the color parameters of the samples showed no obvious change following treatment with 1 M HCl and ethanol for 24 and 72 h (Table 2), indicating the excellent solvent resistance of the hybrid pigments.

Study of the Reversible Acid/Base Allochroic Behavior of ACN/Mnt Hybrid Pigments

The ACN/Mnt hybrid pigments exhibited different colors in HCl and NH_3 atmospheres (Table 3, Fig. 4a). The ACN/Mnt hybrid pigments were dark pink after exposure to an acidic atmosphere, and then changed to dark blue following conversion in an alkaline environment. This reversible color response appeared through at least four acid/base cycles with every cycle lasting 6 min (Fig. 4a). No obvious changes in the chromaticity parameters of hybrid pigments were found after four color-transformation cycles compared with those of the first acid or base cycles (Table 3). In addition, the visible absorption spectra of ACN/Mnt hybrid pigments after the first acid/base cycle were applied to investigate further the color change (Fig. 4b).

Table 2. Color parameters of ACN/Mnt hybrid pigments before and after immersion in 1 M HCl and ethanol for 24 h and 72 h, respectively

Medium	Color parameters (24 h)			Color parameters (72 h)		
	L^*	a^*	b^*	L^*	a^*	b^*
Before immersion	29.02	25.33	–13.02	29.02	25.33	–13.02
1 M HCl	26.75	32.08	–2.17	25.18	29.46	–2.22
Ethanol	27.70	21.44	–13.83	27.93	18.72	–13.55

Table 3. Color parameters of ACN/Mnt hybrid pigments after the first and the fourth acid/base cycles

Samples	Color parameters (HCl)			Color parameters (NH_3)		
	L^*	a^*	b^*	L^*	a^*	b^*
First cycle	31.27	33.33	–6.17	25.37	2.46	–19.95
Fourth cycle	30.69	29.94	–5.48	24.57	3.22	–18.23

In an acidic atmosphere, ACN/Mnt had an absorption band in the visible region (at ~530 nm). On the contrary, with exposure to an NH_3 atmosphere, the wavelength of the absorption-generated bathochrome shifted from 530 to 580 nm, consistent with previous reports (Khaodee et al. 2014; Ogawa et al. 2017). The allochroic responses of hybrid pigments under acidic or alkaline atmospheres were ascribed mainly to the structural transformation of ACN molecules under different atmospheres between the flavylium cation and the quinonoidal base under acid and base conditions, respectively (Fig. 5) (Brouillard and Dubois 1977; Li et al. 2019a,b). The result also suggested that incorporation of Mnt successfully protected the structure of natural ACN molecules from the external environment.

Study of Chemical and Mechanical Properties and the Acidichromism Behavior of ACN/Mnt/SA Smart Films

The chemical interaction between ACN/Mnt and the SA matrix was evaluated by FTIR analysis of films (Fig. 6a). In the FTIR spectrum of SA films, the absorption peaks at 3242, 1597, and 1406 cm^{-1}, as well as at 1025 cm^{-1} were assigned to stretching of the –OH groups, to symmetric and asymmetric stretching of the –COO– groups, and to stretching vibrations of the C–O–C groups, respectively (Ding et al. 2019; Huang et al. 2018). With increase in the amount of ACN/Mnt hybrid pigments from 2 to 4 to 6 wt.%, the –OH stretching bands in ACN/Mnt/SA composite films shifted to 3247, 3248, and 3249 cm^{-1} compared with SA film, which may be ascribed to hydrogen-bond interaction between ACN/Mnt hybrid pigments and the SA matrix (Huang et al. 2018; Kang et al. 2018; Koosha and Hamedi 2019; Zhai et al. 2017).

The mechanical properties of SA and ACN/Mnt/SA composite films were evaluated by studying the tensile strength and elongation at break after five sets of parallel measurements (Fig. 6b, c). After incorporation of 2 wt.% ACN/Mnt, the tensile strength of ACN/Mnt/SA film was similar to that of SA films. With increasing amounts of the ACN/Mnt hybrid pigment, the tensile strength of the composite films increased, and the elongation at break decreased compared to that of SA films. The composite films incorporated with ACN/Mnt showed greater tensile strength, which was attributed to the uniform dispersion and the formation of hydrogen bonds between hybrid pigments and SA (Alboofetileh et al. 2014). Similar

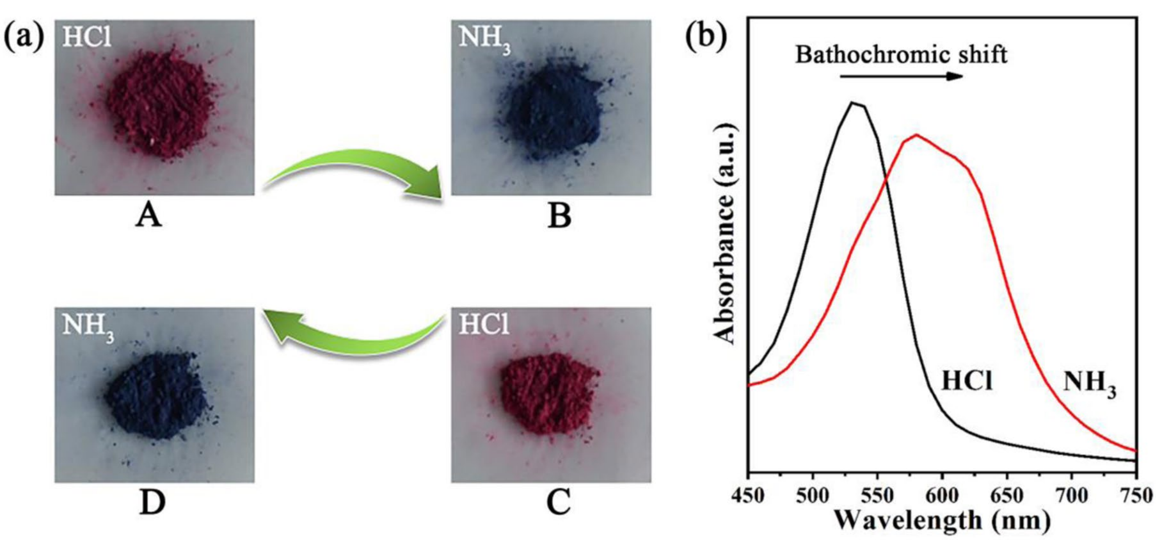

Fig. 4. **a** Images of ACN/Mnt hybrid pigments after the first (A and B) and the fourth (C and D) acid/base cycles; **b** the absorption spectra of ACN/Mnt hybrid pigments after the first acid/base cycles

https://doi.org/10.1007/s42860-021-00114-z Published online by Cambridge University Press

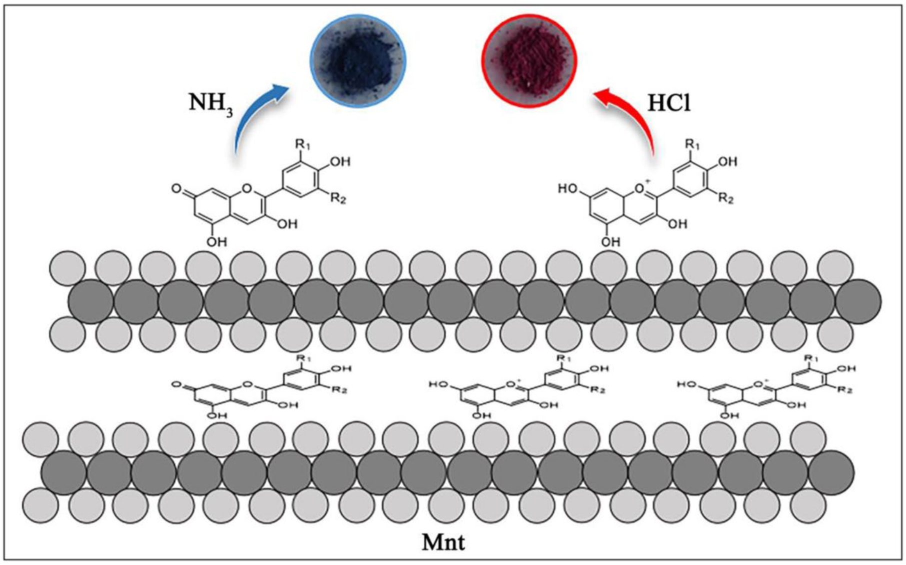

Fig. 5. Structural configuration of ACN molecules adsorbed on the surface and inserted into the interlayer of Mnt under NH_3 or HCl atmospheres (R1, R2 = H, OH, OCH3), and the digital photos of ACN/Mnt hybrid pigments in alkaline (blue circle) and acidic (red circle) atmospheres.

phenomena were also observed for chitosan/polyvinyl alcohol composite films with black carrot ACN (black carrot is a new kind of carrot rich in water-soluble ACN) and bentonite incorporated (Koosha and Hamedi 2019). Increasing the addition of hybrid pigments may yield a small number of aggregates, resulting in a slight reduction in the tensile strength of ACN/Mnt/SA films containing 6 wt.% ACN/Mnt (Ding et al. 2019; Li et al. 2019a). The composite films also had smaller values for elongation at break than the raw films; the decrease was related to the fact that the addition of hybrid pigments restricted the motion of the SA matrix, which led to the disruption of the films (Alboofetileh et al. 2014; Luchese et al. 2018; Qin et al. 2019) .

The color responses of the SA and ACN/Mnt/SA films were evaluated following alternating exposure to HCl (acidic) and NH_3 (alkaline) vapors (Figs. 7, S2). The raw ACN/Mnt/SA composite films containing various amounts of ACN/Mnt began to turn pink after exposure to the acidic atmosphere for 1.5 h (Fig. 7a), but the raw SA film exhibited no such color response (Fig. 7b). In the alkaline atmosphere, the above ACN/Mnt/SA composite films changed from pink to light blue (Fig. S2). Interestingly, the light blue of the biodegradable composite films returned to pink when reexposed to HCl (Fig. S2). The chromogenic degree of biodegradable composite films was directly proportional to the hybrid pigment content, which exhibited potential use for detecting food spoilage.

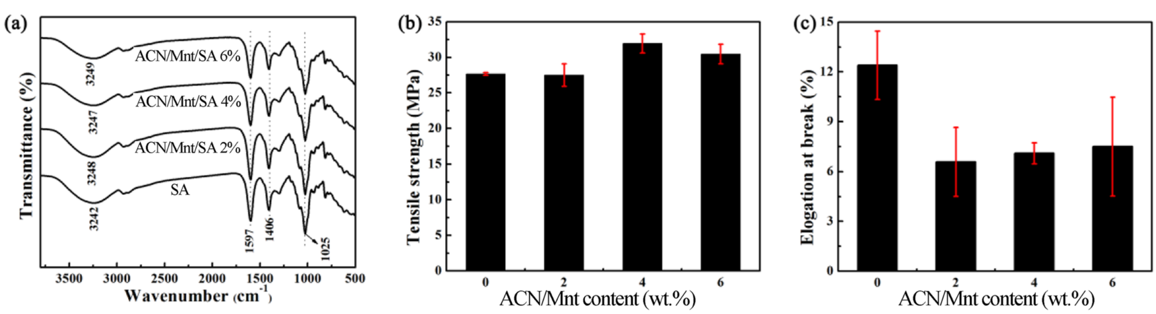

Fig. 6. **a** FTIR spectra, **b** tensile strength, and **c** elongation at break of SA films and ACN/Mnt/SA films containing various amounts of ACN/Mnt

https://doi.org/10.1007/s42860-021-00114-z Published online by Cambridge University Press

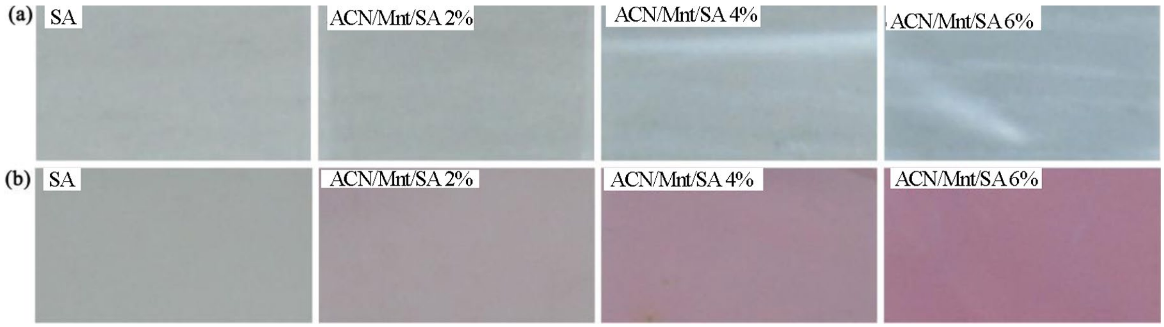

Fig. 7. Digital images showing the colors of SA films and ACN/Mnt/SA films with various amounts of ACN/Mnt **a** before and **b** after exposure to an acidic atmosphere

CONCLUSIONS

In the current study, the possible loading mechanism and the chemical and thermal stability of ACN/Mnt hybrid pigments were investigated. The results showed that ACN was adsorbed on the surface and intercalated into the interlayer of Mnt via electrostatic interaction and cation exchange, and the incorporation into Mnt obviously enhanced the weathering resistance of ACN molecules in various environments. More importantly, the composite films containing ACN/Mnt hybrid pigment exhibited good mechanical properties, and reversible acidichromism behavior compared with SA films. The intelligent composite films appeared pink and light blue following exposure to an acidic or alkaline environment, respectively. Therefore, the biodegradable composite films with both reinforced and reversible allochroic properties could be used in the field of food testing and packaging.

ACKNOWLEDGMENTS

This work was supported financially by the Major Projects of the Natural Science Foundation of Gansu, China (18JR5RA001), the Youth Innovation Promotion Association of the Chinese Academy of Sciences (2017458), the Funds for Creative Research Groups of Gansu, China (17JR5RA306) and the Major Projects of Science and Technology of Gansu, China (17ZD2GA018).

Funding

Funding sources are as stated in the Acknowledgments.

Declarations

Conflict of Interest

The authors declare that they have no conflict of interest.

REFERENCES

Alboofetileh, M., Rezaei, M., Hosseini, H., & Abdollahi, M. (2014). Effect of nanoclay and crosslinking degree on the properties of alginate-based nanocomposite film. *Journal of Food Processing and Preservation, 38,* 1631–1622.

Brouillard, R., & Dubois, J. E. (1977). Mechanism of the structural transformations of anthocyanins in acidic media. *Journal of the American Chemical Society, 99,* 1359–1364.

Cai, X. R., Du, X. F., Cui, D. M., Wang, X. N., Yang, Z. K., & Zhu, G. L. (2019). Improvement of stability of blueberry anthocyanins by carboxymethyl starch/xanthan gum combinations microencapsulation. *Food Hydrocolloids, 91,* 238–245.

Cao, L., Sun, G. H., Zhang, C. J., Liu, W. B., Li, J., & Wang, L. J. (2019). An Intelligent film based on cassia gum containing bromothymol blue-anchored cellulose fibers for real-time detection of meat freshness. *Journal of Agricultural and Food Chemistry, 67,* 2066–2074.

Castañeda-Ovando, A., Pacheco-Hernández, M. D. L., Páez-Hernández, M. E., Rodríguez, J. A., & Galán-Vidal, C. A. (2009). Chemical studies of anthocyanins: A review. *Food Chemistry, 113,* 859–871.

Chiou, C. T., & Rutherford, D. W. (1997). Effects of exchanged cation and layer charge on the sorption of water and egme vapors on montmorillonite clays. *Clays and Clay Minerals*, *45*, 867–880.

Choi, I., Lee, J. Y., Lacroix, M., & Han, J. (2017). Intelligent pH indicator film composed of agar/potato starch and anthocyanin extracts from purple sweet potato. *Food Chemistry, 218,* 122–128.

Ding, J. J., Huang, D. J., Wang, W. B., Wang, Q., & Wang, A. Q. (2019). Effect of removing coloring metal ions from the natural brick-redpalygorskite on properties of alginate/palygorskite nanocomposite film. *International Journal of Biological Macromolecules, 122,* 684–694.

Fang, Z. X., Zhao, Y. Y., Warner, R. D., & Johnson, S. K. (2017). Active and intelligent packaging in meat industry. *Trends in Food Science & Technology, 61,* 60–71.

Fedenko, V. S., Shemet, S. A., & Landi, M. (2017). UV-vis spectroscopy and colorimetric models for detecting anthocyanin-metal complexes in plants: An overview of in vitro and in vivo techniques. *Journal of Plant Physiology, 212,* 13–28.

Ferrage, E. (2016). Investigation of the interlayer organization of water and ions in smectite from the combined use of diffraction experiments and molecular simulations. A review of methodology, applications, and perspectives. *Clays and Clay Minerals, 64,* 346–371.

Guillermin, D., Debroise, T., Trigueiro, P., de Viguerie, L., Rigaud, B., Morlet-Savary, F., Balme, S., Janot, J. M., Tielens, F., Michot, L., Lalevee, J., Walter, P., & Jaber, M. (2019). New pigments based on carminic acid and smectites: A molecular investigation. *Dyes and Pigments, 160,* 971–982.

Gutiérrez, T. J., Ponce, A. G., & Alvarez, V. A. (2017). Nanoclays from natural and modified montmorillonite with and without added blueberry extract for active and intelligent food nanopackaging materials. *Materials Chemistry and Physics, 194,* 283–292.

Huang, D. J., Zhang, Z., Ma, Z. H., & Quan, Q. L. (2018). Effect of natural nanostructured rods and platelets on mechanical and water resistance properties of alginate-based nanocomposites. *Frontiers in Chemistry, 6,* 635.

Kang, S. L., Wang, H. L., Guo, M., Zhang, L. D., Chen, M. M., Jiang, S. W., Li, X. J., & Jiang, S. T. (2018). Ethylene-vinyl alcohol copolymer-montmorillonite multilayer barrier film coated with mulberry anthocyanin for freshness monitoring. *Journal of Agricultural and Food Chemistry, 66,* 13268–13276.

Khaodee, W., Aeungmaitrepirom, W., & Tuntulani, T. (2014). Effectively simultaneous naked-eye detection of Cu(II), Pb(II), Al(III) and Fe(III) using cyanidin extracted from red cabbage as chelating agent. *Spectrochimica Acta Part A – Molecular and BiomolecularSpectroscopy, 126,* 98–104.

Kohno, Y., Kinoshita, R., Ikoma, S., Yoda, K., Shibata, M., Matsushima, R., Tomita, Y., Maeda, Y., & Kobayashi, K. (2009). Stabilization of natural anthocyanin by intercalation into montmorillonite. *Applied Clay Science, 42,* 519–523.

Kohno, Y., Haga, E., Yoda, K., Shibata, M., Fukuhara, C., Tomita, Y., Maeda, Y., & Kobayashi, K. (2014). Adsorption behavior of natural anthocyanin dye on mesoporous silica. *Journal of Physics and Chemistry of Solids, 75,* 48–51.

Kohno, Y., Kato, Y., Shibata, M., Fukuhara, C., Maeda, Y., Tomita, Y., & Kobayashi, K. (2015). Enhanced stability of natural anthocyanin incorporated in Fe-containing mesoporous silica. *Microporous and Mesoporous Materials, 203,* 232–237.

Koosha, M., & Hamedi, S. (2019). Intelligent Chitosan/PVA nanocomposite films containing black carrot anthocyanin and bentonite nanoclays with improved mechanical, thermal and antibacterial properties. *Progress in Organic Coatings, 127,* 338–347.

Kuswandi, B., Jayus, R., & A., Abdullah, A., Heng, L.Y., & Ahmad, M. . (2012). A novel colorimetric food package label for fish spoilage based on polyaniline film. *Food Control, 25,* 184–189.

Kuswandi, B., & Nurfawaidi, A. (2017). On-package dual sensors label based on pH indicators for real-time monitoring of beef freshness. *Food Control, 82,* 91–100.

Li, S. E., Ding, J. J., Mu, B., Wang, X. W., Kang, Y. R., & Wang, A. Q. (2019a). Acid/base reversible allochroic anthocyanin/palygorskite hybrid pigments: Preparation, stability and potential applications. *Dyes and Pigments, 171,* 107738.

Li, S. E., Mu, B., Wang, X. W., Kang, Y. R., & Wang, A. Q. (2019b). Acomparative study on color stability of anthocyanin hybrid pigments derived from 1D and 2D clay minerals. *Materials, 12,* 3287.

Liu, B., Xu, H., Zhao, H. Y., Liu, W., Zhao, L. Y., & Li, Y. (2017). Preparation and characterization of intelligent starch/PVA films for simultaneous colorimetric indication and antimicrobial activity for food packaging applications. *Carbohydrate Polymers, 157,* 842–849.

Luchese, C. L., Abdalla, V. F., Spada, J. C., & Tessaro, I. C. (2018). Evaluation of blueberry residue incorporated cassava starch film as pH indicator in different simulants and foodstuffs. *Food Hydrocolloids, 82,* 209–218.

Luo, W. H., Ouyang, J. P., Antwi, P., Wu, M., Huang, Z. Q., & Qin, W. W. (2019). Microwave/ultrasound-assisted modification of montmorillonite by conventional and gemini alkyl quaternary ammonium salts for adsorption of chromate and phenol: Structure-function relationship. *Science of the Total Environment, 655,* 1104–1112.

Ma, Q. Y., & Wang, L. J. (2016). Preparation of a visual pH-sensing film based on tara gum incorporating cellulose and extracts from grape skins. *Sensors and Actuators B: Chemical, 235,* 401–407.

Maciel, V. B. V., Yoshida, C. M. P., & Franco, T. T. (2015). Chitosan/pectin polyelectrolyte complex as a pH indicator. *Carbohydrate Polymers, 132,* 537–545.

Madejová, J. (2003). FTIR techniques in clay mineral studies. *Vibrational Spectroscopy, 31,* 1–10.

Madejová, J., Gates, W. P., & Petit, S. (2017). IR Spectra of Clay Minerals. *Developments in Clay Science, 8,* 107–149.

Maqueda, C., Afonso, M. D., Morillo, E., Sánchez, R. M. T., Perez-Sayago, M., & Undabeytia, T. (2013). Adsorption of diuron on mechanically and thermally treated montmorillonite and sepiolite. *Applied Clay Science, 72,* 175–183.

Merino, D., Ollier, R., Lanfranconi, M., & Alvarez, V. (2016). Preparation and characterization of soy lecithin-modified bentonites. *Applied Clay Science, 127–128,* 17–22.

Mihindukulasuriya, S. D. F., & Lim, L. T. (2014). Nanotechnology development in food packaging: A review. *Trends in Food Science & Technology, 40,* 149–167.

Müller, P., & Schmid, M. (2019). Intelligent packaging in the food sector: A brief overview. *Foods, 8,* 16.

Ogawa, M., Takee, R., Okabe, Y., & Seki, Y. (2017). Bio-geo hybrid pigment; clay-anthocyanin complex which changes color depending on the atmosphere. *Dyes and Pigments, 139,* 561–565.

Pereira, V. A., Jr., de Arruda, I. N. Q., & Stefani, R. (2015). Active chitosan/PVA films with anthocyanins from Brassica oleraceae (Red Cabbage) as Time-Temperature Indicators for application in intelligent food packaging. *Food Hydrocolloids, 43,* 180–188.

Puligundla, P., Jung, J., & Ko, S. (2012). Carbon dioxide sensors for intelligent food packaging applications. *Food Control, 25*(1), 328–333.

Qin, Y., Liu, Y. P., Yong, H. M., Liu, J., Zhang, X., & Liu, J. (2019). Preparation and characterization of active and intelligent packaging films based on cassava starch and anthocyanins from Lycium ruthenicum Murr. *International Journal of Biological Macromolecules, 134,* 80–90.

Ramírez, A., Sifuentes, C., Manciu, F. S., Komarneni, S., Pannell, K. H., & Chianelli, R. R. (2011). The effect of Si/Al ratio and moisture on an organic/inorganic hybrid material: Thioindigo/montmorillonite. *Applied Clay Science, 51,* 61–67.

Realini, C. E., & Marcos, B. (2014). Active and intelligent packaging systems for a modern society. *Meat Science, 98,* 404–419.

Riaz, M., Zia-Ul-Haq, M., & Saad, B. (2016). Biosynthesis and stability of anthocyanins. In R. W. Hartel (Ed.), *Anthocyanins and Human Health: Biomolecular and therapeutic aspects* (pp. 50–150). Springer, Dordrecht, The Netherlands.

Ribeiro, H. L., Brito, E. S., Souza, M. D. M., & Azeredo, H. M. C. (2018a). Montmorillonite as a reinforcement and

color stabilizer of gelatin films containing acerola juice. *Applied Clay Science, 165,* 1–7.
Ribeiro, H. L., de Oliveira, A. V., de Brito, E. S., Ribeiro, P. R. V., Souza Filho, M. S. M., & Azeredo, H. M. C. (2018b). Stabilizing effect of montmorillonite on acerola juice anthocyanins. *Food Chemistry, 245,* 966–973.
Silva-Pereira, M. C., Teixeira, J. A., Pereira-Júnior, V. A., & Stefani, R. (2015). Chitosan/corn starch blend films with extract from Brassica oleraceae (red cabbage) as a visual indicator of fish deterioration. *LWT-Food Science and Technology, 61,* 258–262.
Silva, G. T. M., da Silva, K. M., Silva, C. P., Rodrigues, A. C. B., Oake, J., Gehlen, M. H., Bohne, C., & Quina, F. H. (2019). Highly fluorescent hybrid pigments from anthocyanin- and red wine pyranoanthocyanin-analogs adsorbed on sepiolite clay. *Photochemical & Photobiological Sciences, 18,* 1750–1760.
Silvestre, C., Duraccio, D., & Cimmino, S. (2011). Food packaging based on polymer nanomaterials. *Progress in Polymer Science., 36,* 1766–1782.
Suchithra, P. S., Vazhayal, L., Mohamed, A. P., & Ananthakumar, S. (2012). Mesoporous organic-inorganic hybrid aerogels through ultrasonic assisted sol-gel intercalation of silica-PEG in bentonite for effective removal of dyes, volatile organic pollutants and petroleum products from aqueous solution. *Chemical Engineering Journal, 200–202,* 589–600.
Trigueiro, P., Rodrigues, F., Rigaud, B., Balme, S., Janot, J. M., dos Santos, I. M. G., Fonseca, M. G., Osajima, J., Walter, P., & Jaber, M. (2018). When anthraquinone dyes meet pillared montmorillonite: Stability or fading upon exposure to light? *Dyes and Pigments, 159,* 384–394.
Wang, G. F., Wang, S., Sun, Z. M., Zheng, S. L., & Xi, Y. F. (2017). Structures of nonionic surfactant modified montmorillonites and their enhanced adsorption capacities towards a cationic organic dye. *Applied Clay Science, 148,* 1–10.
Wang, Y. W., Luan, G. X., Zhou, W., Meng, J., Wang, H. L., Hu, N., & Suo, Y. R. (2018). Subcritical water extraction, UPLC-Triple-TOF/MS analysis and antioxidant activity of anthocyanins from *Lycium ruthenicum* Murr. *Food Chemistry, 249,* 119–126.
Xie, W., Gao, Z. M., Pan, W. P., Hunter, D., Singh, A., & Vaia, R. (2001). Thermal degradation chemistry of alkyl quaternary ammonium montmorillonite. *Chemistry of Materials, 13,* 2979–2990.
Zhai, X. D., Shi, J. Y., Zou, X. B., Wang, S., Jiang, C. P., Zhang, J. J., Huang, X. W., Zhang, W., & Holmes, M. (2017). Novel colorimetric films based on starch/polyvinyl alcohol incorporated with roselle anthocyanins for fish freshness monitoring. *Food Hydrocolloids, 69,* 308–317.
Zhai, X. D., Li, Z. H., Shi, J. Y., Huang, X. W., Sun, Z. B., Zhang, D., Zou, X. B., Sun, Y., Zhang, J. J., Holmes, M., Gong, Y. Y., Povey, M., & Wang, S. Y. (2019). A colorimetric hydrogen sulfide sensor based on gellan gum-silver nanoparticles bionanocomposite for monitoring of meat spoilage in intelligent packaging. *Food Chemistry, 290,* 135–143.
Zhang, Y., Wang, W. B., Mu, Q. W., & Q., & Wang, A. Q. . (2015). Effect of grinding time on fabricating a stable methylene blue/palygorskite hybrid nanocomposite. *Powder Technology, 280,* 173–179.

(Received 3 January 2020; revised 12 February 2021; AE: Chun Hui Zhou)